



The effect of cooling conditions on Ti 6%Al 4%V microstructure observed using high-temperature in-situ scanning electron microscopy

Genevieve A. Kane^{1,2}, Dustin Andersen^{1,2}, M. David Frey², Robert Hull^{1,2,a)}

- ¹Department of Materials Science and Engineering, Rensselaer Polytechnic Institute, 110 8th Street, Troy, NY 12180, USA
- ² Center for Materials, Devices and Integrated Systems, Rensselaer Polytechnic Institute, 110 8th Street, Troy, NY 12180, USA

Received: 2 September 2020; accepted: 22 December 2020; published online: 20 January 2021

This study focuses on continuous imaging of microstructural changes in Ti 6% Al 4% V when cooling from the β transus of ~995 °C or above. A range of microstructures were obtained by accessing different cooling rates. With cooling rates of 0.1–0.5 °C/s, lamellar microstructures were observed, which initiate in a colony microstructure below temperatures of ~930 °C. When the lamellar microstructure began forming at grain boundaries, cooling was interrupted to further observe the kinetics in the system. Lamellae changed in projected length from 40 µm to ~160–320 µm over three minutes at ~930 °C, within the $\alpha + \beta$ mixed phase. On further time at temperature, the lengthening of lamellae stagnated. With further cooling at 0.1 °C/s, lamellae grew in projected width, while the projected length remained the same. In addition, a surface topography formed at elevated temperatures (around 800 °C), evolved during the α to β heating transition, and persisted upon cooling.

Introduction

Ti 6% Al 4% V (Ti 6–4) has both α (hcp) and β (bcc) phases. Above 995 °C (the β transus), only the β phase is thermodynamically stable. Upon cooling from above the β transus, three characteristic microstructures may be formed during the development of the α phase: fully lamellar, basketweave, and martensitic, or a combination thereof.

Fully lamellar microstructures form in colonies at cooling rates of less than 2 °C/s. These lamellar colonies form selecting one of the 12 orientation variants of the $(110)_{\beta}||(0002)_{\alpha}$ Burger's orientation relationship[1], the lowest energy interface between the two phases. In this paper, we define basketweave microstructures as those which form with cooling rates greater than 2 °C/s, during which lamellae can nucleate within the grain itself on different crystallographically equivalent planes. These lamellae are typically of a higher aspect ratio than those found in fully lamellar microstructures. With cooling rates above 3.5 °C/s and the appropriate composition present, martensitic phases can form from the β phase. Martensitic phase transformations can create both α , a hexagonal structure, and α which is orthorhombic [2], depending on the chemical composition, cooling rate, and heat treatment temperature of β prior to cooling [3].

Traditional processing of Ti 6–4 involves the iteration of multiple distinct thermomechanical steps to produce a desired microstructure and the corresponding mechanical properties. These steps generally begin with the homogenization of material above the β transus temperature. Deformation and recrystallization steps can be performed in the $\alpha+\beta$ mixed phase regime and during further annealing of the material at lower temperatures [4]. The combination of hot working and heat treatment allow a variety of two-phase $\alpha+\beta$ microstructures to form [5]. The resulting microstructures can impact material properties such as yield strength and fracture toughness. These properties are controlled by grain size, microstructure morphologies and dimensions, and the volume fraction of α and β [6, 7].

To our knowledge, in-situ scanning electron microscope (SEM) observations of microstructures formed by cooling from temperatures above the β transus in Ti 6–4 have not been previously reported. Studies by Boehlert et al. targeted tensile deformation studies up to 480 °C and at room temperature [8], and Li et al. reported studies of tension-creep behavior of Ti 6–4 and Ti 3%Al 3.5%V at temperatures of 455 °C [9, 10]. The work of Alabort et al. employed maximum temperatures of 900 °C for insitu SEM investigations into superplasticity [11, 12]. Walley et al.

^{a)} Address all correspondence to this author. e-mail: hullr2@rpi.edu



utilized instrumentation that was stated to be capable of heating to 1200 °C but employed a maximum reported temperature of 700 °C for observing creep in nickel-based superalloys [13].

This study explores the real-time microstructural evolution of Ti 6–4 when cooling from above the β transus by real-time imaging in-situ in an SEM. Imaging is performed using a secondary electron (SE) Everhart–Thornley (ET) detector for all subsequent results unless otherwise noted. Each sample is heated at 100 °C per minute to 1200 °C using a proportional-integral-derivative (PID) temperature controller (labeled "Controller" in subsequent temperature curves), with a type R thermocouple ("Heater TC") placed within the cover of the heater, and with a type R thermocouple that is spot welded to the sample surface ("Sample TC"). This allows for the homogenization of β grains, followed by direct observation of the nucleation and growth of α lamellae into the existing β matrix upon cooling.

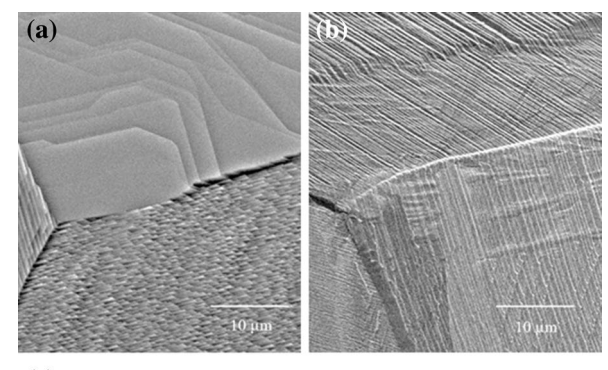
Heating / cooling sequences are shown in Table 1, together with the maximum temperature attained as measured by the Sample TC. Note that although the controller was set to the nominal maximum of 1200 °C for each iteration of the experiments, the maximum sample TC temperature that was recorded varied according to the exact assembly of the heater components for each experiment. Grain size statistics are taken as an average of the spacing between intersections of grain boundaries with 6 lines across the horizontal field width of the images. The horizontal field width of each image for this analysis was 2 mm. Grain sizes are taken at room-temperature post-cooling, as well as before thermal processing.

Results

Formation of periodic surface topography

The existence of a periodic surface topography is observed in all experiments, as initially described in Kane et al. [14] where

the topography is observed to form during heating at approximately 930 °C and persists throughout the subsequent temperature sequences. Figure 1a shows surface topography within the β grain at the lower right of the image, while the sample is held at 1060 °C. Figure 1b shows an image of the same location when the sample is cooled below 200 °C. Figure 1c indicates the temperature vs time conditions for the experiment. It is noted that



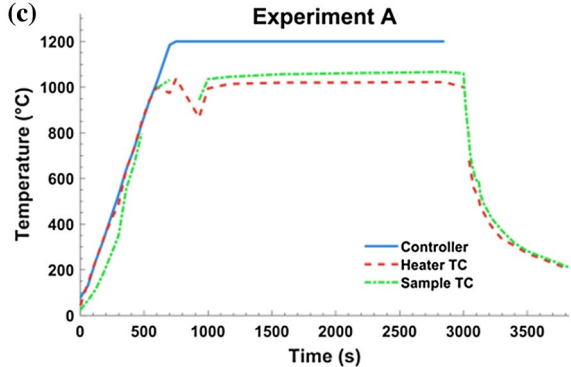


Figure 1: Experiment A (a) Periodic topography imaged after 40 min at 1060 °C with 20 keV primary beam energy; (b) periodic topography post-cooling imaged at 5 keV primary beam energy. (c) Temperature–time curve for Experiment A.

TABLE 1: Heating/cooling sequences employed.

Experiment	Temperature maximum (sample TC) (°C)	Hold Time (minutes)	Cooling rate (°C/s)	Additional information	Grain size after heat treatment (µm)
A	1060	40	Radiative Cooling	NA	1000
В	970	30	0.1	NA	600
C	1100	0	Radiative Cooling	NA	400
D	1100	30	0.5	NA	700
E	1100	0, 45	0.1	Sample held at 950 °C to examine lamellar formation	375

A Sample annealed to a maximum temperature of 1060 °C, held for 40 min, and then radiatively cooled; B Sample annealed to a maximum temperature of 970 °C, held for 30 min, and then cooled at 0.1 °C/s using PID Control; C Sample annealed to a maximum temperature of 1100 °C and then immediately radiatively cooled; D Sample annealed to a maximum temperature of 1100 °C, held for 30 min, and then cooled at 0.5 °C/s; E Sample annealed to a maximum temperature of 1100 °C, cooled at 0.1 °C/s, and held at 950 °C for 45 min to observe lamellar microstructure formation, followed by additional cooling at 0.1 °C/s. All temperatures are those determined from the Sample TC. Starting average grain size is 30 μ m.



shortly before reaching the β transus in this experiment, the temperature measured on the heater and sample TCs drop. We occasionally have observed such temperature glitches when the temperature reaches its maximum, and suspect it is associated with the current limit and controller in the heating apparatus. However, as it is transient and short in duration, it should not affect the microstructural evolution significantly.

Figure 2 shows the formation of periodic topography as the sample temperature is ramped up during Experiment B. Figure 2a is imaged 360 s into the experiment at 752 °C during heating and continues showing a lamellar microstructure similar to the pre-anneal structure. At 794 °C (30 s later), we observe in Fig. 2b initiation of periodic topography. Figure 2c shows the topography has further developed at 968 °C, and that the bimodal microstructure has fully dissolved by this temperature, approximately 10 min into the experiment.

Figure 3 shows an atomic force microscope (AFM) amplitude scan of the periodic surface topography, and a corresponding SEM image from the same location, from Experiment E described later in the document. The period of the topography is around 300 nm and is around 100 nm in amplitude in this instance.

In Fig. 3, the period of the topography on the bottom right of the image (within an α phase lamella) is greater than on the

top left of the image (in the β phase). In a mixed phase region containing an α lamellae, the period of topography increases by a factor of 2 or 3. We observe this generally across all experiments.

The impact of cooling rate on transverse and lateral lamellar growth

Three different cooling rates were used to investigate lamellar growth rates. Figure 4 shows the microstructure in Experiment C after completion of the temperature sequence shown in Fig. 4g, using radiative cooling (3-4 °C/s). Figure 4a, b shows a grain boundary triple junction after cooling to room temperature, in which a basketweave structure is present in all grains. Lower magnification images in the left column show variations in the characteristic size of the basketweave microstructures from grain to grain, much like the lamellar colonies seen at slower cooling rates. The variation in the length of the lamellar components of the basketweave structure within neighboring grains can be seen in Fig. 4c, d vs e, f. As experiments are performed without the ability to tilt the sample, we acknowledge that there are stereological effects associated with the measurements. Specifically, with the twelve geometrical variants associated with the lamellae habit planes, the width and length of a given lamellae are not known, because of uncertainty in the

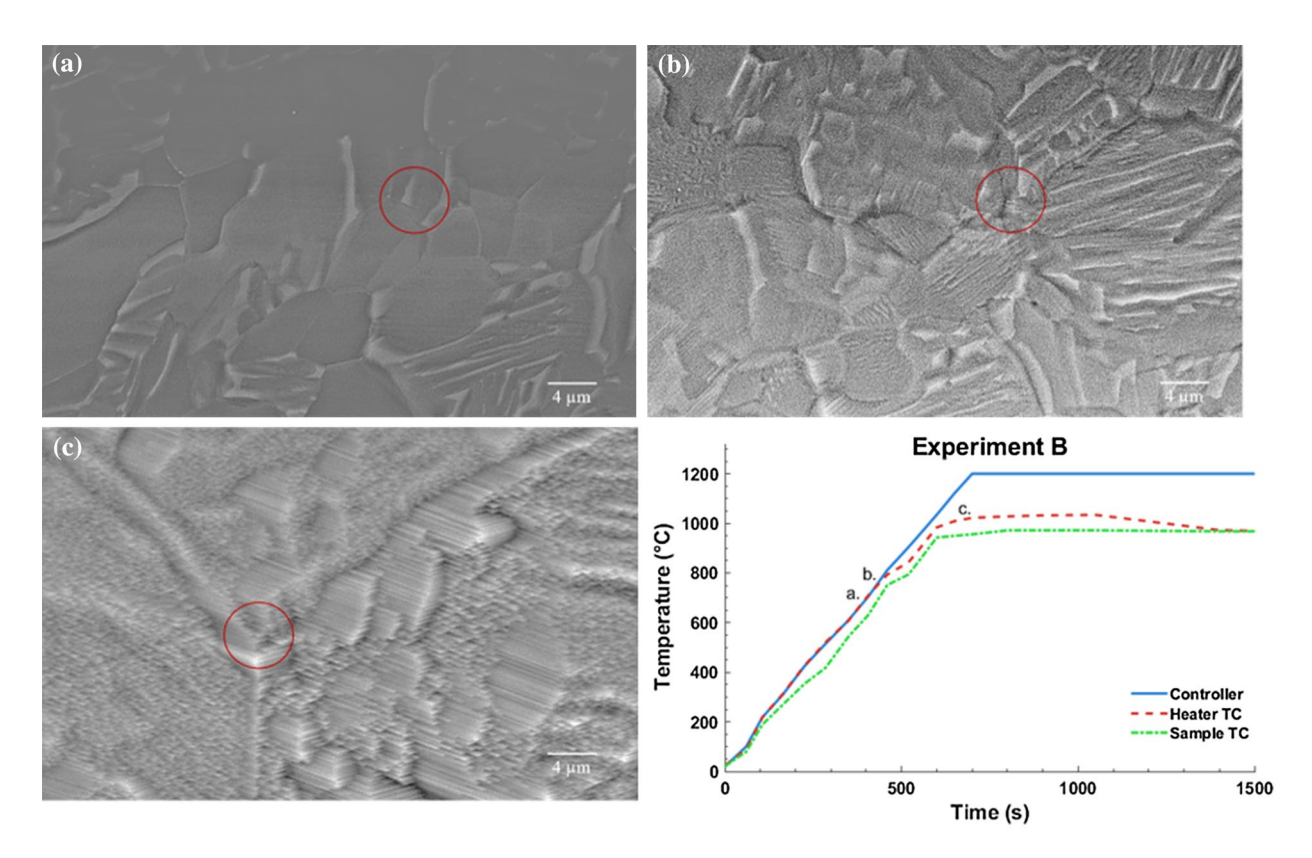


Figure 2: Microstructure evolution for Experiment B. (a) Microstructure at 752 °C during heating ramp, (b) continued heating ramp at 794 °C, (c) after reaching the maximum temp of 968 °C. All images taken with primary beam energy of 20 keV. Circles indicate the same location in each image.



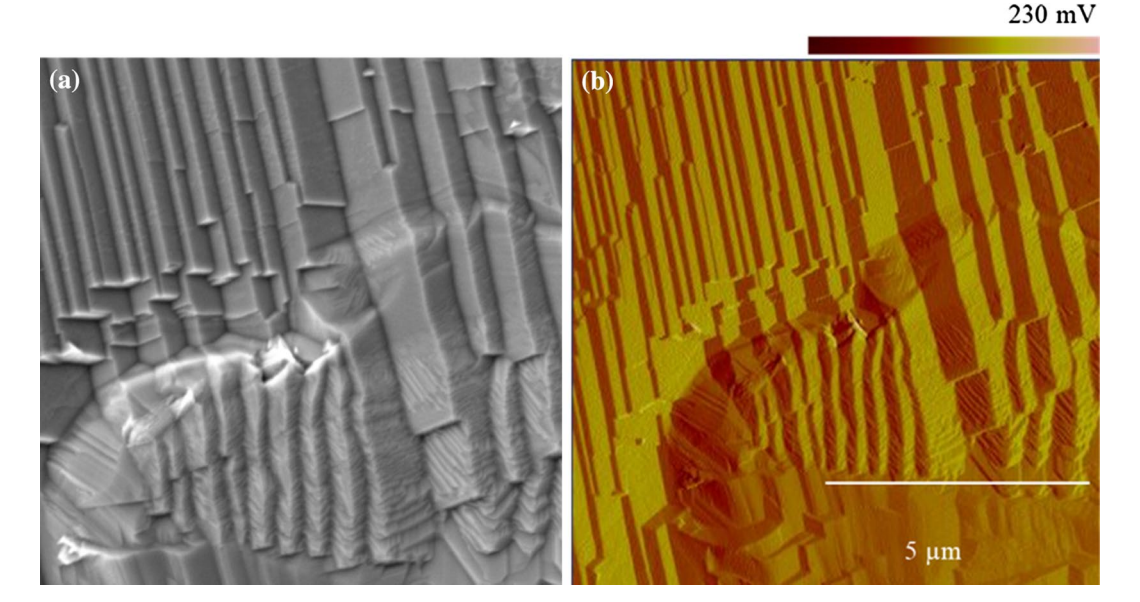


Figure 3: (a) Surface topography imaged in an SEM following Experiment E conditions, taken with 5 keV primary beam energy. (b) AFM amplitude scan from the same area.

orientation of the habit plane with respect to the sample surface. We thus describe projected lamellae widths and lengths in the subsequent results, and emphasize relative versus absolute changes in dimensions. The projected dimensions of the lamellar components are around 8 μm wide and around 24 μm long in Fig. 4c, d but around 4–6 μm wide and 16 μm long in Fig. 4e, f.

Figure 5 shows results from Experiment D, performed with a cooling rate of 0.5 °C/s. Figure 5a shows the nucleation of lamellae from a grain boundary, at a temperature of 940 °C and at projected lamellar lengths of 10–20 μm . Figure 5b taken 20 s later shows lamellar growth to $\sim 20-40~\mu m$ in projected length (during a ~ 10 °C drop in temperature). An additional 10 s and 5 °C temperature drop leads to the lamellae doubling in projected length to 80–120 μm in Fig. 5c. Figure 5d shows additional lamellar microstructure forming in neighboring grains after an additional 10 s (with a ~ 5 °C drop in temperature). Here, lamellae range in projected length from 80 to 160 μm . Beyond this time, we see stagnation in the lengthening of lamellae. Figure 5e shows the final microstructure upon cooling to 100 °C.

In Experiment E, with sample cooling at a rate of 0.1 °C/s, we examine how fast lamellae grow while held at the initial nucleation temperature of 946 °C (as determined by the sample TC), as well as the impact of cooling on the aspect ratio of the lamellae. In our previous work [14], lamellae in this sample were shown to grow from 40–160 μ m in projected length (the nucleation event was not captured) to 80–320 μ m in projected length at 946 °C during imaging over a period of 3 min. At this time, lamellar growth stopped, often with no observable microstructural features such as grain boundaries impeding the growth. Figure 6 further details the evolution of lamellae during cooling

in this sample. A low magnification image taken at the start of cooling is shown in Fig. 6a. Figure 6b shows a region where the α lamellae are 3.5 to 7 μm in projected width during cooling from 946 to 940 °C. Figure 6c shows that the resulting projected width of the lamellar structure arrests at around 8 to 15 μm at 494 °C (4500 s into the cooling cycle.). Figure 6d shows the microstructure near the end of cooling at 445 °C (5000 s into the cooling cycle). The lamellae double in width, showing an overall projected aspect ratio change (length:width) of \sim 25:1 to \sim 12:1 from \sim 940 to 445 °C.

Discussion

Periodic topography

We were unable to find previous reports of the periodic surface topography we observe in Ti 6–4. A possible reason for this is that in most papers in the literature, samples are generally polished after annealing and cooling, prior to imaging in an electron microscope, thus removing any fine surface topography. The topography we observe forms during heating at temperatures around 800 °C, where the microstructure is still predominantly α , and reorients when α lamellae dissolve into the β matrix (at around 930 °C), presumably because of the different crystallography of the α and β grains. It is then largely stable through subsequent heating and cooling. The direction of the topography is consistent throughout each grain but varies depending upon the grain it is observed in. The period and orientation of the topography are uniform from the temperature of formation, up to the maximum



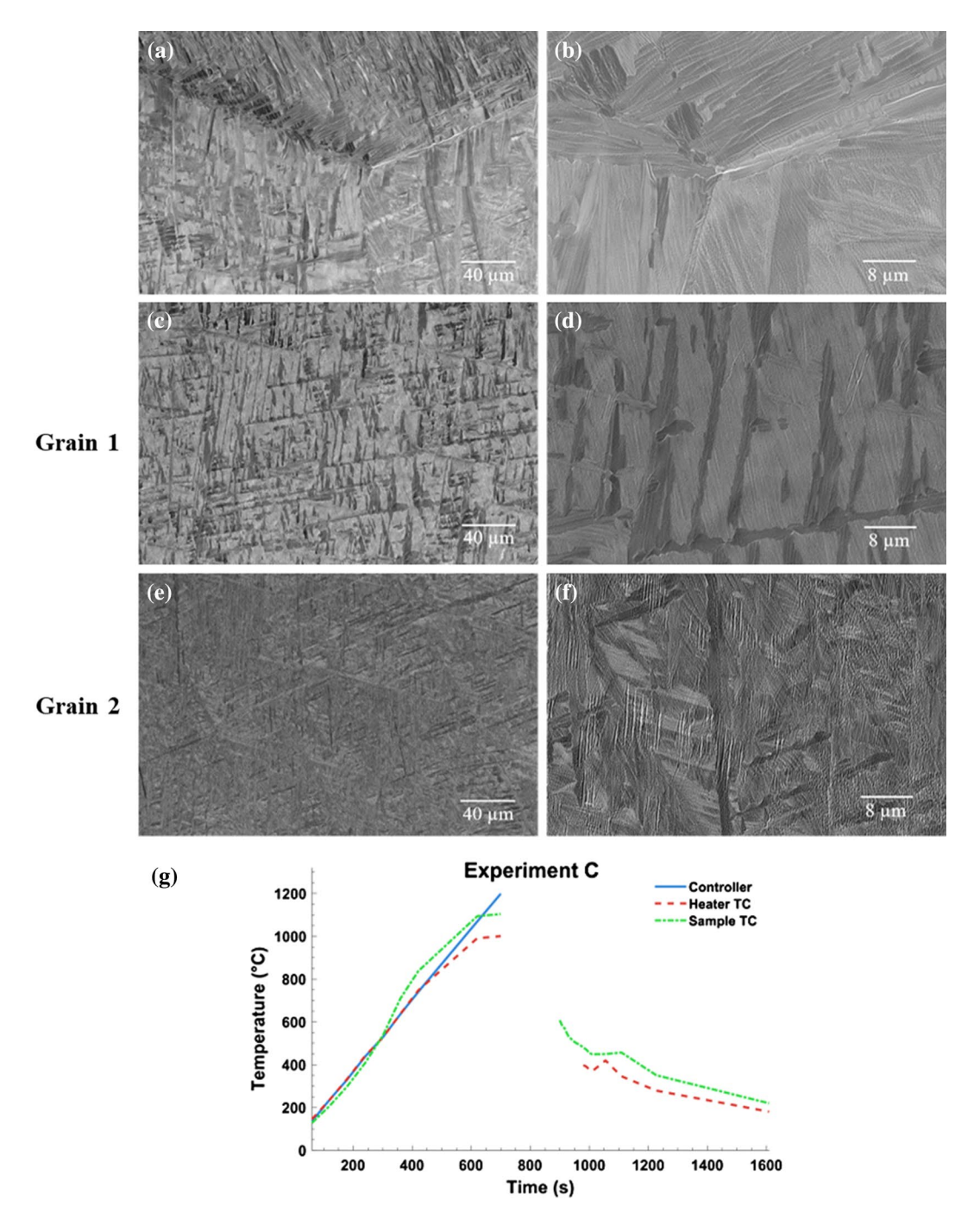


Figure 4: Microstructure after cooling to room temperature for Experiment C conditions. (a and b) Low- and high-magnification images of microstructure around a triple junction. (c and d) Basketweave microstructure within a grain at low- and high-magnification images. (e and f) Low- and high-magnification images of basketweave microstructure in a different neighboring grain. (g) Temperature–time curve for this experiment. All images taken with a 5 keV primary beam energy. Note that discontinuity in cooling curve occurs was due to a momentary heater stage controller malfunction but will not affect the radiative cooling process.

temperature in our experiments (1100 °C). The topography only changes in period upon cooling through 930 °C, in regions where lamellae nucleate and grow.

The only superficially similar topographical features we found in literature were in the superplasticity study by Alabort

[11], attributed to shear banding at elevated temperatures of $\sim\!700$ °C and strain rates of 10^{-4} s $^{-1}$. The shear bands in Alabort's elevated temperature study have a minimum period of $\sim\!2~\mu m$ and do not occur throughout each grain [12]. The topography seen in the experimental results in this paper does not occur



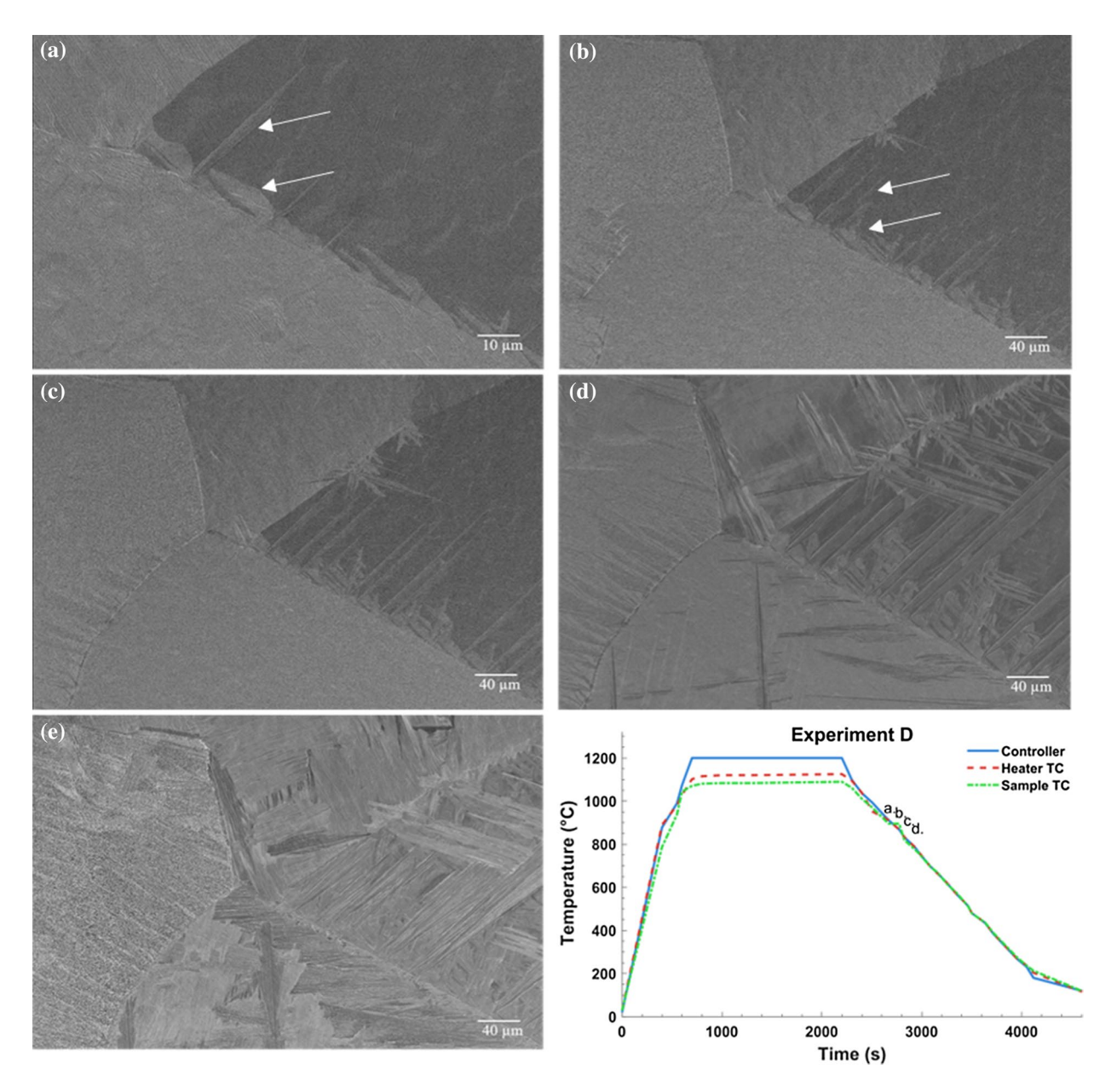


Figure 5: Microstructure evolution during cooling with Experiment D conditions in Table 1. Images recorded at (a) 940 °C (b) 930 °C (c) 925 °C (d) 920 °C (e) 100 °C. Secondary electron images taken at 5 keV. Arrows indicate the growing α lamellae.

under applied strain, nor does it have similar periodicity. Rather we believe that the surface topography is surface faceting that occurs to reduce the surface energy at the Ti 6–4 to vacuum interface.

While we could find no reports of surface faceting in the literature for Ti 6–4, it is a well-studied phenomenon in other materials systems [15–17]. The basic principle behind surface faceting is that different faces (e.g., exposed planes) of a crystal have different surface energies associated with them, and given time and adequate thermal energy [18], the surface will rearrange topographically[19], increasing the crystal

surface area, but decreasing the total surface energy by exposing low energy facets. The surface facets would be distinct for α and β in this system, because of the different crystallography of the two phases. Thus, while the facets initially form in the mixed phase during heating, as the α phase dissolves into the β phase, at around 930 °C, it is to be expected that the orientation of the surface faceting changes, as we observe. The topography is stable while the microstructure remains predominantly β , but on subsequent cooling below the β transus, nucleation and growth of the α phase would be expected to modify the topography. The ability to re-orient



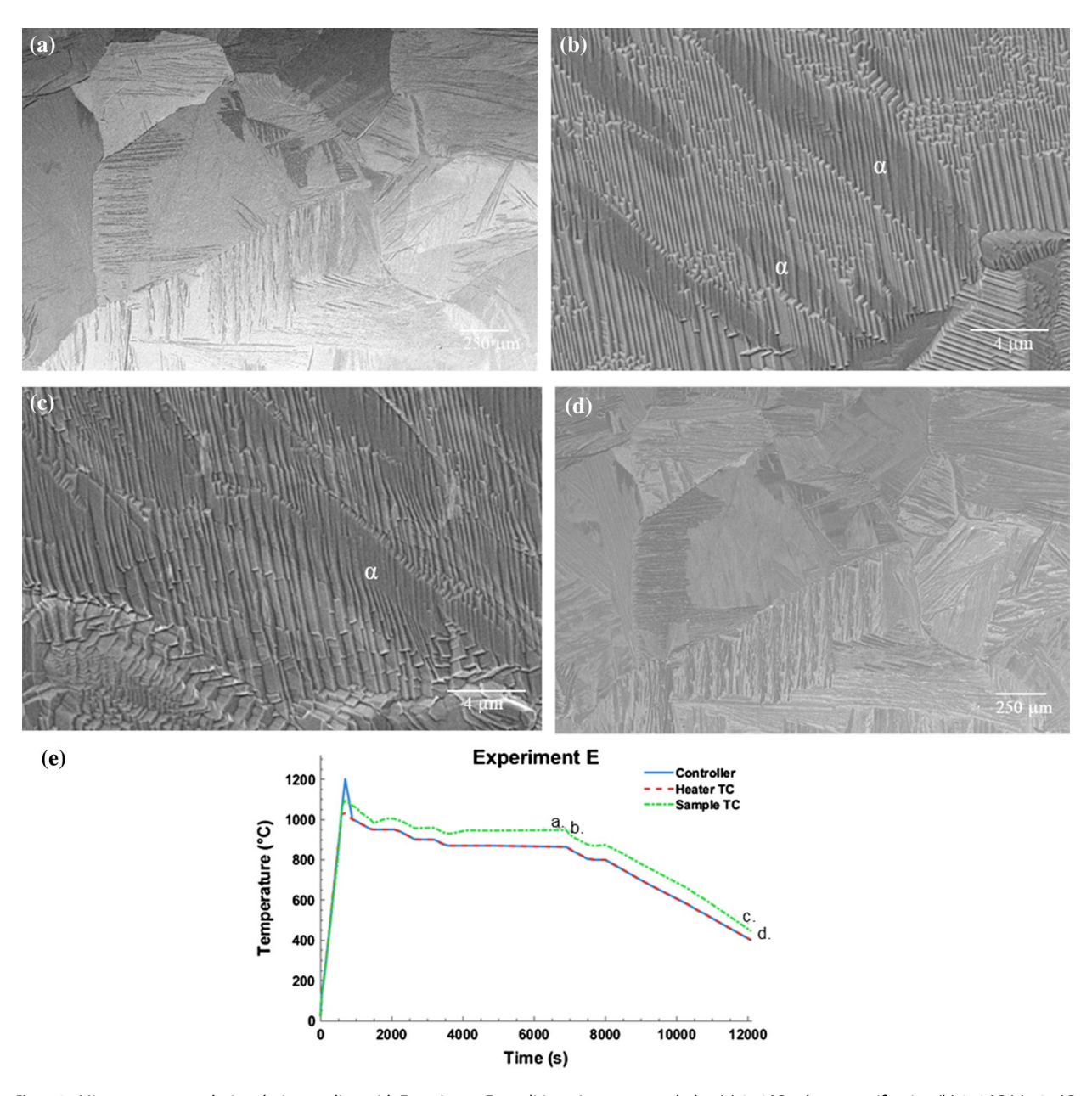


Figure 6: Microstructure evolution during cooling with Experiment E conditions. Images recorded at (a) 946 °C at low magnification (b) 940 °C (c) 494 °C (d) after cooling to 445 °C. All images taken at 5 keV. In images, α lamellae are annotated accordingly. (e) Temperature–time curve.

the topography to adapt to the different crystallography of the α phase would depend on the adatom mobility and, thus, the time at temperature, which is defined by the cooling rate. In practice, we observe that as α lamella form, the topography changes mainly in period (by a factor of 2-3x) in the mixed phase regions, rather than in orientation (for example, as seen in Fig. 3), presumably due to the finite cooling rates. The volume change while heating from α to β , and cooling to α again may also affect the faceting of the exposed surface as strain, as well as temperature, has been shown to drive surface faceting [20–22].

Surface and bulk microstructure comparison

We next consider how the distribution of the phases at the surface (which is what we observe in our real-time SEM studies) might differ from the bulk of the material. Figure 7 shows a cross-sectional image of the sample from an experiment where the sample was annealed above the β transus for 40 min, then radiatively cooled. While we acknowledge that different atomic diffusivities at the surface versus the bulk may impact observations of lamellar growth in our secondary electron images, no discernible systematic changes in lamellar microstructure or phase concentrations are observed in the surface versus the



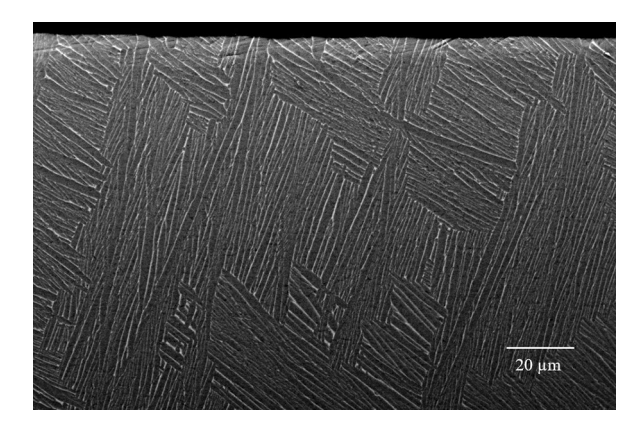


Figure 7: SEM image of cross section of post-annealed microstructure, showing uniform distribution of β (bright features) near surface and within bulk of material. Changes in contrast near the top edge are likely due to rounding of the edges of the sample from polishing. Backscattered electron image taken with 20 keV primary electron beam energy. Sample was annealed above the β transus for 40 min, then radiatively cooled

bulk in cross-sectional images, such as Fig. 7 and other higher magnification images. Figure 7 additionally demonstrates the absence of α case formation (a surface layer in which the α phase is stabilized by oxygen diffusion from the surface into the bulk of Ti 6–4), since oxygen has been reported to be an α stabilizer [23]. For example, Brice et al. [23] furnace annealed Ti 6-4 in atmosphere at 950 °C for 25 h and 50 h creating 40 µm and 80 μm thick α case regions, respectively. While the annealing temperature of 950 °C is similar to our study, the annealing times are significantly longer than ours (1 h maximum). More significantly, we perform annealing at the SEM vacuum level of 10⁻⁵ torr, which will reduce arrival rates of oxygen on the surface of the sample by about 8 orders of magnitude compared to atmospheric pressure and thus drastically reduce the adsorption and diffusion of oxygen into the material [24, 25]. Based on the reduced time at temperature and oxygen adsorption, we would expect an a case thickness that does not significantly affect our observations.

Lamellar growth in Ti 6-4

The growth and dissolution of lamellar microstructure in Ti 6-4 are described in multiple sources in the literature, e.g., [26-29], but we are not aware of prior studies of real-time observations of growth and nucleation of lamellae within Ti 6-4. Such real-time studies allow us to analyze how lamellae nucleate and grow as a function of thermal treatment. This work shows that lamellar microstructures lengthen quickly after nucleation, increasing in aspect ratio (length: width) but eventually stagnate in length when held at a constant temperature for an extended time. The lamellae only grow measurably in width during cooling cycles, not when held isothermally at temperatures where significant

lengthening occurs. We note that projected lengths of lamellae are only directly comparable in a given colony, due to the stereological effects described earlier.

In the recent comprehensive work by Ackerman et al. [30], lamellar growth in a somewhat different composition alloy, Ti-6Al-2Sn-4Zr-6Mo, was studied in detail experimentally and by modeling, where their modeling results were extended to other alloys such as Ti 6–4. For the Ti-6Al-2Sn-4Zr-6Mo system, their experimental samples were heated above the β transus by passing a direct current through the sample, rapidly cooled from above the β transus to a holding temperature of 800–900 °C for 5–50 min, and then water quenched. In measurements taken after quenching and sectioning, it was inferred that lamellae grew tenths of microns per minute during the holding period. This agreed with Ackerman et al.'s analytical velocity modeling predictions (using established diffusion equations, thermodynamic data calculated by commercial software, and lamellar geometry as inputs) in Table 1 of reference 30.

In our work in Ti 6–4, we measure a projected lamellar growth velocity (length) on the order of 10 μ m/min when held at 948 °C (Experiment E), while Ackerman et al.'s models predict a growth velocity for Ti 6–4 of 1.32 μ m/min at 900 °C in Table 1 of reference 30. Their model further predicts that the velocity would decrease at temperatures closer to the β transus, such as in our experiments at 948 °C.

In comparing our measurements to those of Ackerman et al., which are inferred from post-quench, final microstructures, we make the following points: (i) We acknowledge that stereological effects in our observations (as discussed earlier) mean that for lamellae whose growth front are inclined to the surface, the projected velocity we observe is necessarily greater than the actual lamellar growth velocity. (ii) In our observations, lamellae grow rapidly after nucleation and then stagnate after a few minutes. Thus, if we were to infer velocities in our work from longer anneal times, we would underestimate the velocity while growth is actually occurring. (iii) Related to point (ii), inspection of figures such as Fig. 7 in Ackerman et al. (consistent with our own observations) suggests that lamellar growth is terminated relatively quickly by intersection with other microstructural features such as grain boundaries or lamellae in different orientations. In fact, in our in-situ observations, we see a relatively narrow time window where lamellar growth occurs unimpeded by other microstructural features. In summary, these points illustrate the power of in-situ, real-time methods: microstructural observations can be made continuously, and variations in kinetic processes such as lamellar growth can be continuously observed.

Figure 8 shows the projected lamellar length versus time for a constant temperature of 946 °C (Experiment E) and with cooling rates of 0.1 °C/s from a maximum temperature of 968 °C (Experiment B) and 0.5 °C/s with a starting temperature of 940 °C (Experiment D). In both Experiments B and E, doubling



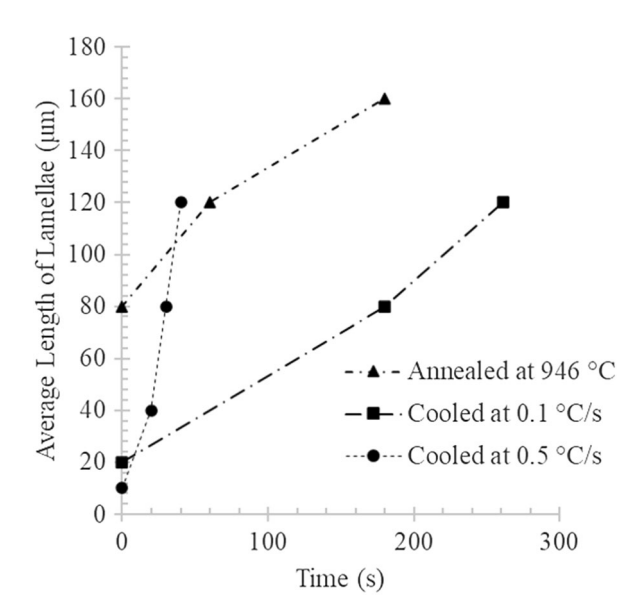


Figure 8: Average projected length of lamellae versus time for Experiment B (Cooled at 0.1 °C/s from a maximum temperature of 968 °C); Experiment E (annealed isothermally at 946 °C); and Experiment D (Cooled at 0.5 °C/s from a temperature of 940 °C).

of the projected length of the lamellae occurs on the order of minutes (corresponding to a projected growth rate of $20{-}30~\mu\text{m/}$ min), whereas the projected length of lamellae in Experiment D doubles in just 10 s corresponding to a projected growth rate of over $100~\mu\text{m/min}$). This is consistent with a greater undercooling at the faster cooling rate, as discussed below. In contrast, the average projected growth rate in width of lamellae is in the range of tenths of μm per minute (e.g., doubling from 4 to 8 μm over 4000 s cooling from 946 °C at 0.1 °C/s, Experiment E). In fact, in Experiment E, we do not see any observable widening during the 45 min anneal at 946 °C, prior to cooling.

These observations are consistent with a competition between the thermodynamic driving force to create the α phase upon cooling below the β transus, and the diffusivity of Al and V atoms (the stabilizing elements for α and β phases, respectively). Greater undercooling (determined by the cooling rate) increases the growth rate of the α phase, until reduced diffusion becomes the limiting factor [31]. At a slow cooling rate, the system has time to fully equilibrate its α fraction and requires further cooling to drive the growth of more α . At fast cooling rates, the system cannot equilibrate fast enough to accommodate the increased driving force for greater α fraction.

The lowest energy interface $((110)_{\beta}||(0002)_{\alpha})$ within Ti 6–4 leads to 12 orientation variants for α lamellae in the β matrix. The reduction of the number of α variants (and thus lamellae orientations) is to be expected for slower cooling, due in part to the preference for growth over nucleation for smaller degrees of undercooling [32]. The relatively fewer lamellae at lower cooling rate tend to nucleate in colonies,

because one variant will have the lowest activation energy at a given local orientation of a grain boundary. At high rates of cooling, nucleation becomes more preferred relative to growth, leading to a larger number of smaller α lamellae, and increasing the number of α variants, and thus a microstructure that is more characteristic of basketweave.

This demonstrates how in-situ SEM observations can provide a more detailed understanding of the processing conditions that lead to a desired microstructure. In particular, we have shown here how lamellar aspect ratios may be controlled. Several reports [33–35] have shown significant changes in ductility, fracture toughness, and crack growth mechanisms in Ti 6–4 as a function of the size and shape of α phase (in particular, equiaxed versus lamellar microstructure). For example, fully lamellar microstructures are shown to be more resistant to growth of macro-scale cracks, since the α/β lamellae interface may deflect the crack path, increasing crack tortuosity, crack tip shielding, and crack tip closure.

Conclusions

We have provided new insight into the lamellar growth in Ti 6–4 using in-situ heating techniques in the SEM, while imaging in real time during cooling from above the β transus temperature. At cooling rates of 0.1 °C/s and 0.5 °C/s from temperatures below about 940 °C where lamellae first nucleate, they initially lengthen (at ten times the rate for 0.5 °C/s versus 0.1 °C/s) and then cease growth in length in the span of minutes. They continue to widen on further cooling, reducing the projected lamellar aspect ratio. Utilizing such measurements, specific aspect ratios and densities of lamellae may be engineered. This can impact material property optimization, for example, in terms of macro- and micro-crack propagation in Ti 6–4, as discussed above.

A novel surface topography was observed to form while the sample was heating at around 800 °C. This topography initiates when the microstructure is still predominately α , however by around 930 °C, when the α phase has largely dissolved into the β matrix, it is reoriented according to the new crystal structure. This topography is consistent with surface faceting. The periodicity of the surface topography then changes as α lamellae grow during cooling. The existence of this topography, and its inter-relationship with the underlying phase structure, could be significant in affecting the evolution of microstructure at the surface.

Methods

A Zeiss Crossbeam dual scanning electron and focused ion beam microscope is integrated with a heating-stressing-indentation stage created by Kammrath & Weiss GmbH [36]. The



stage (shown in Fig. 9) is capable of heating the sample to a maximum of 1200 °C, with radiative cooling rates averaging around 3–4 °C/s in the temperature range of 1100 to 500 °C, where most microstructural evolution is observed. Cooling rates below the radiative cooling rate are controlled by a PID controller. The radiative cooling rate of 3–4 °C/s was chosen to observe basketweave microstructure formation, while controlled cooling rates of 0.5 and 0.1 °C/s were chosen to observe lamellar microstructure formation.

A complete description of sample preparation for the Ti 6–4 (Grade 5) samples is described in Kane et al. [14]. Sample dimensions are shown in Fig. 9, where the length, width, and thickness post-mechanical polishing are 24 mm, 2.5 mm, and 1.5 mm, respectively. The beginning microstructure is bi-modal, seen in Fig. 9b, with the β phase appearing brighter in this image due to the difference in secondary electron yields between the phases. In general, we are able to discern between grains during high-temperature imaging due to channeling contrast, from variations in the SE2 secondary electrons that are generated from backscattered electrons. Additional contrast at the grain boundaries may be due to thermal etching at high annealing temperatures, as described in Heard et al. [37].

We cannot directly identify α and β phases with the signals we have available at high temperature; however, during the insitu experiments, we cool from above the β transus, allowing for unambiguous identification of α lamellae as they form. Further, in post-mortem analysis, we were able to confirm the identity of β and α phases in the same imaged regions as those studied at high temperature through backscattered electron imaging and energy dispersive x-ray spectroscopy (EDS) mapping.

The SEM setup uses a 25 mm working distance to mitigate the effects of stage heating on detectors and columns, as well as to accommodate the stage size and geometry.

Images were captured with field widths of $60 \mu m$, $300 \mu m$, and 2 mm to utilize sufficient spatial resolution to determine microstructural features and to ensure a sufficient field of view to allow statistically meaningful observations to be drawn. As described earlier, the temperature is defined by the PID temperature controller ("Controller") and measured by thermocouples at the heater ("Heater TC") and the sample ("Sample TC").

Cooling rates are either the maximum attainable cooling rate from radiative cooling, or a controlled lower cooling rate of 0.1–0.5 °C/s, as set by the PID controller. These cooling rates encompass the conditions for formation of lamellar and basketweave microstructures, but not martensitic structures [6].

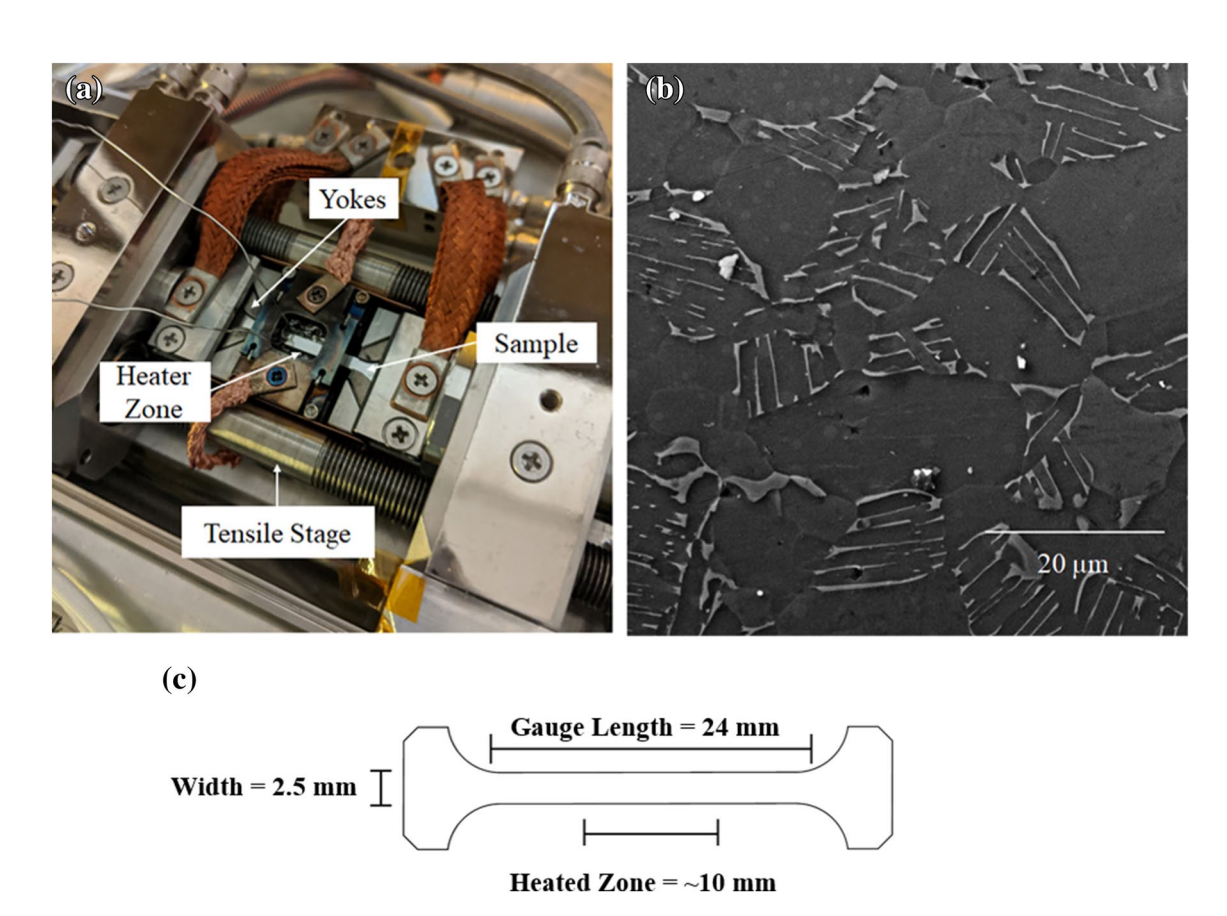


Figure 9: (a) Image of thermomechanical stage. (b) Initial bi-modal microstructure of as-recieved Ti 6–4 samples taken at 5 keV primary beam energy prior to heating. (c) Schematic of the sample.



During cooling, a temperature change of 5–10 °C occurs during the SE image capture time for the experiments shown which are cooled at 0.1–0.5 °C/s.

Acknowledgments

We acknowledge the sponsorship of the National Science Foundation, through CMMI-1647005 (equipment design and construction) and CMMI-1729336 (in-situ experimentation in Ti 6-4) awards for funding this work, as well as the use of characterization and cleanroom facilities within the Center for Materials, Devices and Integrated Systems at Rensselaer Polytechnic Institute. We acknowledge Brent Engler for useful discussions on lamellar growth. In addition, we acknowledge Konrad Weiss, Farhad Ghaleh, and George Lanzarotta from Kammrath and Weiss GmbH., for their expertise and assistance with equipment development.

References

- 1. G. Lütjering, Influence of processing on microstructure and mechanical properties of $(\alpha+\beta)$ titanium alloys. Mater. Sci. Eng. A. **243**, 32–45 (1998)
- S.L. Semiatin, V. Seetharaman, I. Weiss, Hot workability of titanium and titanium aluminide alloys—an overview. Mater. Sci. Eng. A. 243, 1–24 (2002)
- Y.T. Lee, M. Peters, G. Welsch, Elastic moduli and tensile and physical properties of heat-treated and quenched powder metallurgical Ti-6Al-4V alloy. Metall. Trans. A. 22, 709–714 (1991)
- G. Lütjering, Property optimization through microstructural control in titanium and aluminum alloys. Mater. Sci. Eng. A. 263, 117–126 (1999)
- N. Poondla, T.S. Srivatsan, A. Patnaik, M. Petraroli, A study of the microstructure and hardness of two titanium alloys: Commercially pure and Ti-6Al-4V. J. Alloys Compd. 486, 162–167 (2009)
- S.L. Semiatin, S.L. Knisley, P.N. Fagin, F. Zhang, D.R. Barker, Microstructure evolution during alpha-beta heat treatment of Ti-6Al-4V. Metall. Mater. Trans. A 34, 2377–2386 (2003)
- 7. S. Patil, S. Kekade, K. Phapale, S. Jadhav, A. Powar, A. Supare, R. Singh, Effect of α and β phase volume fraction on machining characteristics of titanium alloy Ti6Al4V. Procedia Manuf. **6**, 63–70 (2016)
- C.J. Boehlert, C.J. Cowen, S. Tamirisakandala, D.J. McEldowney, D.B. Miracle, In situ scanning electron microscopy observations of tensile deformation in a boron-modified Ti-6Al-4V alloy. Scr. Mater. 55, 465-468 (2006)
- H. Li, C.J. Boehlert, T.R. Bieler, M.A. Crimp, Analysis of the deformation behavior in tension and tension-creep of

- Ti-6Al-4V(wt%) at 298K and 728K using in-situ SEM experiments. Philos. Mag. **95**, 691–729 (2015)
- H. Li, C.J. Boehlert, T. Bieler, M.A. Crimp, Analysis of the deformation behavior in tension and tension-creep of Ti-3Al-25V (wt pct) at 296 K and 728 K (23 °C and 455 °C) using in situ SEM experiments. Metall. Mater. Trans. A 45(13), 6053–6066 (2014)
- E. Alabort, D. Putman, R.C. Reed, Superplasticity in Ti-6Al-4V: characterisation, modelling and applications. Acta Mater. 95, 428–442 (2015)
- E. Alabort, P. Kontis, D. Barba, K. Dragnevski, R.C. Reed, On the mechanisms of superplasticity in Ti-6Al-4V. Acta Mater. 105, 449-463 (2016)
- J.L. Walley, R. Wheeler, M.D. Uchic, M.J. Mills, In-situ mechanical testing for characterizing strain localization during deformation at elevated temperatures. Exp. Mech. 52, 405–416 (2012)
- G.A. Kane, D.M. Frey, R. Hull, Influence of controlled cooling rates during thermal processing of Ti 6% Al 4% V alloys using insitu scanning electron microscopy. MRS Adv. 5, 1603–1611 (2020)
- L. Vitos, A.V. Ruban, H.L. Skriver, J. Kollár, The surface energy of metals. Surf. Sci. 411, 186–202 (1998)
- G. Bilalbegovic, F. Ercolessi, E. Tosatti, High-temperature surface faceting. Surf. Sci. Lett. 258, L676–L678 (1991)
- P. Wynblatt, D. Chatain, Surface segregation anisotropy and equilibrium shape of alloy crystals. Rev Adv Mater Sci. 21, 44 (2009)
- E.D. Williams, N.C. Bartelt, Surface faceting and the equilibrium crystal shape. Ultramicroscopy 31, 35–48 (1989)
- 19. J.R. Heffelfinger, C.B. Carter, Mechanisms of surface faceting and coarsening. Surf. Sci. **389**, 188–200 (1997)
- R. Narayanan, C. Carter, Bunching of surface steps and facet formation on analumina surface. J. Mater. Res. 17, 98–106 (2002)
- 21. R. Verre, R.G.S. Sofin, V. Usov, K. Fleischer, D. Fox, G. Behan, H. Zhang, I.V. Shvets, Equilibrium faceting formation in vicinal ${
 m Al_2O_3}$ (0001) surface caused by annealing. Surf. Sci. **606**, 1815–1820 (2012)
- M.A. Cuddihy, A. Stapleton, S. Williams, F.P.E. Dunne, On cold dwell facet fatigue in titanium alloy aero-engine components.
 Int. J. Fatigue. 97, 177–189 (2017)
- D.A. Brice, P. Samimi, I. Ghamarian, Y. Liu, R.M. Brice, R.F. Reidy, J.D. Cotton, M.J. Kaufman, P.C. Collins, Oxidation behavior and microstructural decomposition of Ti-6Al-4V and Ti-6Al-4V-1B sheet. Corros. Sci. 112, 338–346 (2016)
- 24. B. Sefer, Oxidation and alpha-case phenomena in titanium alloys used in aerospace industry: Ti-6Al-2Sn-4Zr-2Mo and Ti-6Al-4V, Lulea University of Technology, (2014).
- Y. Mizuno, F.K. King, Y. Yamauchi, T. Homma, A. Tanaka,
 Y. Takakuwa, T. Momose, Temperature dependence of oxide decomposition on titanium surfaces in ultrahigh vacuum. J. Vac. Sci. Technol. A 20, 1716 (2002)

- D. Damisih, I. Jujur, J. Sah, D. Prajitno, Effect of heat treatment temperature on microstructure characteristic and hardness properties of casted Ti-6Al-4V ELI. Widyariset. 4, 153–162 (2018)
- 27. S.L. Semiatin, T.M. Lehner, J.D. Miller, R.D. Doherty, D.U. Furrer, Alpha/beta heat treatment of a titanium alloy with a nonuniform microstructure. Metall. Mater. Trans. A 38, 910–921 (2007)
- A. Attanasio, M. Gelfi, A. Pola, E. Ceretti, C. Giardini, Influence of Material Microstructures in Micromilling of Ti6Al4V Alloy. Materials (Basel). 6, 4268–4283 (2013)
- 29. S. Shademan, V. Sinha, A.B.O. Soboyejo, W.O. Soboyejo, An investigation of the effects of microstructure and stress ratio on fatigue crack growth in Ti-6Al-4V with colony α/β microstructures. Mech. Mater. **36**, 161–175 (2004)
- A.K. Ackerman, A.J. Knowles, H.M. Gardner, A.A.N. Nemeth,
 I. Bantounas, A. Radecka, M. Moody, P.A.J. Bagot, R. Reed, D.
 Rugg, D. Dye, The kinetics of primary alpha plate growth in
 titanium alloys. Metall. Mater. Trans. A. 51, 131–141 (2020)
- 31. F.H. Froes, Titanium-physical metallurgy processing, and applications. ASM Int. **20**, 32–33 (2015)

- 32. N. Stanford, P.S. Bate, Crystallographic variant selection in Ti-6Al-4V. Acta Mater. **52**, 5215–5224 (2004)
- 33. J. Tao, S. Hu, L. Ji, Effect of micromorphology at the fatigue crack tip on the crack growth in electron beam welded Ti-6Al-4V joint. Mater. Charact. **120**, 185–194 (2016)
- R.K. Nalla, B.L. Boyce, J.P. Campbell, J.O. Peters, R.O. Ritchie, Influence of microstructure on high-cycle fatigue of Ti-6Al-4V: Bimodal vs lamellar structures. Metall. Mater. Trans. A 33, 899–918 (2002)
- Tiley, J. Modeling of Microstructure Property Relationships in Ti-6Al-4V. Ph.D. Dissertation, The Ohio State University 2002
- Kammrath and Weiss GmbH (2015). https://www.kammrathweiss.com/.
- R. Heard, J.E. Huber, C. Siviour, G. Edwards, E. Williamson-Brown, K. Dragnevski, An investigation into experimental in situ scanning electron microscope (SEM) imaging at high temperature. Rev. Sci Inst. 91, 063702 (2020)